The Astrophysical Journal, 704:126–136, 2009 October 10 doi:10.1088/0004-637X/704/1/126

LoCuSS: THE MID-INFRARED BUTCHER–OEMLER EFFECT

C. P. Haines[1], G. P. Smith[1], E. Egami[2], R. S. Ellis[3,4], S. M. Moran[5], A. J. R. Sanderson[1], P. Merluzzi[6], G. Busarello[6], and R. J. Smith[7]

[1] School of Physics and Astronomy, University of Birmingham, Edgbaston, Birmingham, B15 2TT, UK; cph@star.sr.bham.ac.uk
[2] Steward Observatory, University of Arizona, 933 North Cherry Avenue, Tucson, AZ 85721, USA
[3] California Institute of Technology, 105-24 Astronomy, Pasadena, CA 91125, USA
[4] Department of Astrophysics, University of Oxford, Keble Road, Oxford, OX1 3RH, UK
[5] Department of Physics and Astronomy, The Johns Hopkins University, 3400 N. Charles Street, Baltimore, MD 21218, USA
[6] INAF - Osservatorio Astronomico di Capodimonte, via Moiariello 16, I-80131 Napoli, Italy
[7] Department of Physics, Durham University, Durham, DH1 3LE, UK
Received 2009 March 28; accepted 2009 August 14; published 2009 September 21

ABSTRACT

We study the mid-infrared (MIR) properties of galaxies in 30 massive galaxy clusters at $0.02 \leqslant z \leqslant 0.40$, using panoramic *Spitzer*/MIPS 24 μm and near-infrared data, including 27 new observations from the LoCuSS and ACCESS surveys. This is the largest sample of clusters to date with such high-quality and uniform MIR data covering not only the cluster cores, but extending into the infall regions. We use these data to revisit the so-called Butcher–Oemler (BO) effect, measuring the fraction of massive infrared luminous galaxies ($K < K^{\star}+1.5$, $L_{\rm IR} > 5\times10^{10}\,L_{\odot}$) within r_{200}, finding a steady increase in the fraction with redshift from $\sim$3% at $z = 0.02$ to $\sim$10% by $z = 0.30$, and an rms cluster-to-cluster scatter about this trend of 0.03. The best-fit redshift evolution model of the form $f_{\rm SF} \propto (1+z)^n$ has $n = 5.7^{+2.1}_{-1.8}$, which is stronger redshift evolution than that of $L^{\star}_{\rm IR}$ in both clusters and the field. We find that, statistically, this excess is associated with galaxies found at large cluster-centric radii, specifically $r_{500} < r < r_{200}$, implying that the MIR BO effect can be explained by a combination of both the global decline in star formation in the universe since $z \sim 1$ and enhanced star formation in the infall regions of clusters at intermediate redshifts. This picture is supported by a simple infall model based on the Millennium Simulation semianalytic galaxy catalogs, whereby star formation in infalling galaxies is instantaneously quenched upon their first passage through the cluster, in that the observed radial trends of $f_{\rm SF}$ trace those inferred from the simulations. The observed $f_{\rm SF}$ values, however, lie systematically above the predictions, suggesting an overall excess of star formation, either due to triggering by environmental processes, or a gradual quenching. We also find that $f_{\rm SF}$ does not depend on simple indicators of the dynamical state of clusters, including the offset between the brightest cluster galaxy and the peak of the X-ray emission. This is consistent with the picture described above in that most new star formation in clusters occurs in the infall regions, and is thus not sensitive to the details of cluster–cluster mergers in the core regions.

Key words: galaxies: active – galaxies: clusters: general – galaxies: evolution – galaxies: stellar content

Online-only material: color figures

1. INTRODUCTION

The evolution of galaxies in clusters since $z \simeq 1$ is expected to reflect both changes in the raw ingredients, i.e., the properties of galaxies that have fallen into clusters from the field in this time, and the physical processes that have acted on those galaxies after infall. Early evidence for cluster galaxy evolution was presented by Butcher & Oemler (1978, 1984, hereafter BO84), who found that the fraction of cluster members bluer than the cluster red sequence (f_b), by at least $\Delta_{B-V} = 0.2$ mag in the $B-V$ rest frame, increases from zero in the local universe to $\sim$0.2 by $z \simeq 0.4$, implying a rapid evolution of the cluster population over the last 5 billion years. Empirically, the star-forming spiral galaxies found by BO84 at $z \sim 0.2$–0.4 are mostly replaced by S0 galaxies in local clusters (Dressler et al. 1997; Treu et al. 2003). A simple interpretation is that clusters accreted blue gas-rich star-forming spirals at $z \geqslant 0.5$–1 and that these galaxies have been transformed somehow into the passive S0s found in local clusters by having their gas reservoirs depleted by one or more physical processes within clusters, including for example ram pressure stripping, starvation or harassment (for reviews see Boselli & Gavazzi 2006; Haines et al. 2007).

However, more recent studies of the so-called Butcher–Oemler (BO) effect and the evolution of the morphology–density relation have suggested that at least some of the observed evolutions in f_b is due to selection biases. First, BO84 selected galaxies on optical luminosity (M_V) rather than stellar mass (or M_K), and were therefore susceptible to biases arising from low-mass spiral galaxies—the optical luminosities of such galaxies are boosted by starburst activity, and thus they increasingly enter the samples at higher redshifts (De Propris et al. 2003; Holden et al. 2007). Similarly, the use of a fixed Δ_{B-V} and M_V for blue galaxy selection fails to take account of the youth (and thus brightness and blue-ness) of stellar populations in galaxies at higher redshifts relative to their lower redshift counterparts. To counter this effect, Andreon et al. (2006) and Loh et al. (2008) have advocated the use of differential k-corrections to associate blue galaxies with the same spectral classes of galaxies at all redshifts, and to take into account the expected luminosity evolution of galaxies when defining the M_V (or better still M_K) limits. The above studies all conclude that once these selection biases have been eliminated the redshift evolution of f_b is significantly reduced, suggesting that there has been little evolution in the cluster galaxy population since $z \simeq 1$. Similarly, when using mass-selected samples ($\mathcal{M} > 4\times10^{10}\,M_{\odot}$) Holden et al. (2007) and van der Wel et al. (2007) find that the morphological composition of clusters and the morphology–density relation has remained largely unchanged since $z \sim 0.8$,

as opposed to luminosity-selected ($M_V < M_V^\star + 1$) samples where significant redshift evolution is seen (Smith et al. 2005a; Postman et al. 2005; Desai et al. 2007).

Another more subtle bias arises from the selection of the clusters themselves. BO84's cluster sample was a heterogeneous mixture of clusters identified from photographic plates or by their association with radio galaxies, and hence favored the inclusion of more extreme clusters at high redshifts, in particular those with higher blue fractions, as they would be easier to detect and identify. Indeed Newberry et al. (1988) and Andreon & Ettori (1999) showed that the high-redshift clusters of the BO84 sample are much more X-ray luminous and have higher velocity dispersions and central surface densities than their low-redshift counterparts, suggesting that these selection biases could mimic evolutionary effects, and illustrating the need for well-defined samples of clusters spanning a large redshift range. More recent studies of X-ray-selected clusters again find that both the scatter in the blue galaxy fraction and the trend with redshift is much reduced (Smail et al. 1998; Margoniner & de Carvalho 2000; Ellingson et al. 2001; Fairley et al. 2002; Andreon et al. 2006) relative to those measured from optically selected cluster samples (BO84, De Propris et al. 2007; Goto et al. 2003). These latter samples contain a large number of poor clusters, and although the influence of X-ray luminosity (L_X), velocity dispersion (σ) or cluster richness on f_b is still much debated (Margoniner et al. 2001; Wake et al. 2005; Goto et al. 2003; Popesso et al. 2007; Aguerri et al. 2007), there seems a general consensus that for massive ($\sigma > 600\,\mathrm{km\,s^{-1}}$), X-ray luminous clusters there is little scatter or evolution in f_b out to $z \sim 0.8$ (Smail et al. 1998; Homeier et al. 2005; Poggianti et al. 2006; Aguerri et al. 2007).

Finally, the scatter in the blue galaxy fraction among the intermediate-redshift ($0.15 \leqslant z \leqslant 0.3$) clusters is large; values for individual clusters lying in the range $f_b \sim 0{-}0.2$, i.e., values typical of clusters at $z = 0$ and $z = 0.5$, respectively. This has often been broadly attributed to the dynamical status of the clusters, with actively merging clusters showing higher fractions of blue or star-forming galaxies than those apparently relaxed (Miller & Owen 2003; Miller et al. 2005). However, equally this could be due to field galaxy contamination, as the blue galaxy fractions are estimated by statistically subtracting foreground and background objects by comparison to control fields, a process that becomes increasingly uncertain at higher redshifts as the level of field contamination rises. However, in an analysis based on only spectroscopically confirmed members of 60 clusters at $z < 0.11$ covered by the 2dFGRS, De Propris et al. (2007) obtained a similarly large scatter in the blue galaxy fraction, including some clusters with $f_b > 0.4$, and also found no correlations between f_b and other cluster properties including richness, substructure, concentration.

The sensitivity of the *Infrared Space Observatory* and more recently *Spitzer* at mid-infrared (MIR) wavelengths has opened up a new window for studying star formation in galaxy clusters. The most straightforward interpretation (Kennicutt et al. 2007) of the 24 μm emission is that it traces the dust obscured star formation, while the observed UV or Hα emission traces the unobscured one (Calzetti et al. 2007). MIR observations of clusters have revealed a population of dusty star-forming cluster galaxies (e.g., Fadda et al. 2000; Duc et al. 2002; Biviano et al. 2004; Geach et al. 2006; Marcillac et al. 2007; Bai et al. 2009; Dressler et al. 2009; Haines et al. 2008; Saintonge et al. 2008). Indeed, these MIR-detected star-forming galaxies often have optical colors consistent with the passively evolving early-type cluster galaxies (Wolf et al. 2005; Haines et al. 2008) and would therefore be missed by the traditional BO studies. Saintonge et al. (2008) therefore combined the dusty star-forming cluster members, defined here as having MIR star formation rates (SFRs) higher than $5\,M_\odot\,\mathrm{yr}^{-1}$, with the traditionally selected blue cluster members—all found within $R \leqslant 1\,\mathrm{Mpc}$ of the cluster centers—to show that the optical and IR populations contribute roughly equally to the observed BO effect out to $z \simeq 0.8$. However, several studies have shown that the dusty galaxies contribute significantly more to the integrated cluster SFR than the optically selected blue galaxies. For example, SFRs derived from the [O II] emission line are typically $\sim$10–30$\times$ lower than rates estimated from IR luminosities (e.g., Metcalfe et al. 2005; Geach et al. 2009). However, these previous studies have analyzed either single clusters or at most a handful of heterogeneously selected clusters over a large redshift range, with 1–2 clusters per redshift slice, such that no statistical analysis of trends with cluster properties or redshift has yet been done in the MIR.

In this paper, we revisit the BO effect, taking advantage of recently obtained panoramic *Spitzer* MIR and ground-based NIR imaging of 22 clusters at $0.15 \leqslant z \leqslant 0.3$ from LoCuSS (Local Cluster Substructure Survey; http://www.sr.bham.ac.uk/locuss; see also Section 2.1 for more details) plus comparable data for Coma and Abell 1367 at $z = 0.023$, five clusters from the Shapley supercluster at $z = 0.048$ covered by ACCESS (A Complete CEnsus of star formation and nuclear activity in the Shapley Supercluster), and Cl 0024+17 at $z = 0.394$. In contrast to the only previous MIR BO study (Saintonge et al. 2008), our large sample of 30 clusters in total allows us to measure the scatter in the f_{SF}–redshift relation as a function of redshift, and to explore the relationship between the scatter and simple indicators of the dynamical state of the clusters. We also use the very wide field of view of our data to explore the radial dependence of the MIR BO effect out to cluster-centric radii of $R \gtrsim 2\,\mathrm{Mpc}$. In summary, we present a statistical analysis of 30 clusters, aiming to probe the balance between (1) the evolution of field galaxies that fall into clusters, and (2) the physical processes (some of which may be related to cluster–cluster mergers) at play within the clusters, in shaping the population of actively star-forming cluster galaxies.

In Section 2, we summarize the data used in this paper and the photometric analysis. The main results are then presented in Section 3, followed by a summary and discussion in Section 4. Throughout we assume $\Omega_M = 0.3$, $\Omega_\Lambda = 0.7$, and $\mathrm{H}_0 = 70\,\mathrm{km\,s^{-1}Mpc^{-1}}$.

2. DATA

We have assembled a data set on 30 clusters at $0.02 \leqslant z \leqslant 0.4$ with NIR imaging extending out to the infall regions and panoramic *Spitzer*/MIPS 24 μm photometry covering the same regions. Observational details for the clusters are listed in Table 1. New observations of 27 clusters at $z < 0.3$ are described in Sections 2.1 and 2.2 below. The data and photometry for the one remaining cluster at $z = 0.4$ (Cl 0024) were described in detail by Moran et al. (2007) and Geach et al. (2006); in this paper, we make use of the Cl 0024 master catalog[8] and refer the readers to the relevant papers for further details.

[8] Available from http://www.astro.caltech.edu/~smm/clusters.

Table 1
Observational Details of the Cluster Sample

Cluster Name	z	NIR[a]	r_{500} (Mpc)	$N_{\rm gals}$ ($< K^*$+1.5)	$f_{\rm SF}$
Abell 1367	0.022	1	0.83	47	$0.068^{+0.062}_{-0.039}$
Coma	0.023	1	1.50	126	$0.029^{+0.025}_{-0.017}$
Abell 3556	0.048	2	0.70	16	$0.000^{+0.109}_{-0.000}$
Abell 3558	0.048	2	1.29	181	$0.017^{+0.017}_{-0.011}$
Abell 3562	0.048	2	0.91	61	$0.052^{+0.047}_{-0.029}$
SC 1327-313	0.048	2	0.91	128	$0.031^{+0.028}_{-0.020}$
SC 1329-317	0.048	2	0.76	67	$0.051^{+0.039}_{-0.033}$
RXJ1720.1+2638	0.160	3	1.53	183	$0.048^{+0.022}_{-0.016}$
Abell 586	0.171	3	1.15	225	$0.033^{+0.021}_{-0.017}$
Abell 1914	0.171	3	1.56	210	$0.028^{+0.019}_{-0.014}$
Abell 2218	0.174	4	1.26	219	$0.032^{+0.020}_{-0.016}$
Abell 2345	0.176	3	1.05	118	$0.021^{+0.025}_{-0.015}$
Abell 665	0.182	4	1.38	233	$0.049^{+0.023}_{-0.019}$
Abell 1689	0.182	3	1.50	259	$0.043^{+0.018}_{-0.014}$
Z1883/ZwCl 0839.9+2937	0.194	3	1.11	94	$0.095^{+0.044}_{-0.034}$
Z1693/ZwCl 0823.2+0425	0.223	3	1.00	110	$0.031^{+0.034}_{-0.022}$
Abell 2219	0.225	4	1.49	363	$0.043^{+0.016}_{-0.013}$
Abell 1763	0.228	3	1.22	262	$0.036^{+0.020}_{-0.016}$
Abell 2390	0.230	4	1.50	303	$0.073^{+0.027}_{-0.024}$
RXJ2129.6+0005	0.234	3	1.23	238	$0.100^{+0.032}_{-0.028}$
Z2089/ZwCl 0857.9+2107	0.235	4	1.02	57	$0.089^{+0.076}_{-0.056}$
Abell 1835	0.252	3	1.59	392	$0.063^{+0.022}_{-0.020}$
Z348/ZwCl 0104.4+0048	0.254	5	1.00	131	$0.129^{+0.048}_{-0.044}$
Z7160/ZwCl 1454.8+2233	0.258	3	1.13	114	$0.049^{+0.036}_{-0.023}$
Abell 1758S	0.273	3	1.38	189	$0.052^{+0.029}_{-0.023}$
Abell 1758N	0.279	3	1.16	313	$0.053^{+0.021}_{-0.018}$
Abell 689	0.279	3	1.20	180	$0.137^{+0.039}_{-0.033}$
Abell 697	0.283	3	1.51	286	$0.076^{+0.025}_{-0.022}$
Abell 611	0.288	3	1.37	252	$0.126^{+0.025}_{-0.032}$
Cl 0024+17	0.394	6	1.00	149	$0.148^{+0.043}_{-0.038}$

Note.
[a] Source of NIR data: (1) GOLDmine database (Gavazzi et al. 2003); (2) WFCAM K-band data from ACCESS; (3) WFCAM JK-band data from LoCuSS; (4) NEWFIRM JK-band data from LoCuSS; (5) UKIDSS; (6) Treu et al. (2003).

2.1. LoCuSS

LoCuSS is a multi-wavelength survey of a morphologically unbiased sample of 100 X-ray luminous galaxy clusters at $0.15 \leqslant z \leqslant 0.3$ drawn from the *ROSAT* All Sky Survey cluster catalogs (Ebeling et al. 1998, 2000; Böhringer et al. 2004). The overall aim is to constrain the cluster-to-cluster scatter in the observable properties (e.g., X-ray temperature, integrated SZ-effect Y-parameter, SFR, far-infrared galaxy luminosity function) of massive clusters at low redshift, and to interpret these observables in the context of hierarchical assembly, aided by gravitational lensing probes of the distribution of dark matter in the clusters (e.g., Smith & Taylor 2008). These analyses will, for example, deliver new constraints both on the normalization, shape, and scatter of mass-observable scaling relations required for precision cluster cosmology, and on the evolutionary pathways of gas-rich field galaxies into passive cluster early-type galaxies. Early results on these two complementary aspects of the survey can be found in Zhang et al. (2008), Marrone et al. (2009), and Haines et al. (2009).

The first batch of 30 clusters in our survey benefits from a particularly rich data set, including: Subaru/Suprime-Cam optical imaging (Okabe et al. 2009), *Spitzer*/MIPS 24 μm maps, GALEX near- and far-ultraviolet (NUV/FUV) imaging, and near-infrared (NIR; J, K) imaging from UKIRT/WFCAM and KPNO-4m/NEWFIRM. All of these data embrace at least a half-degree field of view centered on each cluster, and thus probe the clusters out to ∼1–2 virial radii. We have also been awarded 500 ks on *Herschel* as an Open Time Key Programme to observe this sample at 100 and 160 μm with PACS. These 30 clusters were selected from the parent sample simply on the basis of being observable by Subaru on the nights allocated to us. In principle, these 30 should therefore not suffer any gross biases toward one type of cluster or another (e.g., cool core cluster, merging cluster, etc.). In this paper, we analyze the 22 clusters from the full sample of 30 for which both NIR and MIR data are in-hand.

2.1.1. LoCuSS Mid-IR Observations

Each cluster was observed across a $25' \times 25'$ field of view at 24 μm with MIPS (Rieke et al. 2004) on board the *Spitzer Space Telescope*[9] (Werner et al. 2004), consisting of a 5×5 grid of MIPS pointings in fixed cluster or raster mode (PID: 40872; PI: G.P. Smith). At each grid point, we performed two cycles of the small-field photometry observations with a frame time of 3 s, producing a total per pixel exposure time of 90 s. The central $5' \times 5'$ tile of some clusters had already been imaged by Guaranteed Time Observations Program 83 to a much deeper depth (∼3000 s pixel^{-1}); these data were combined with our 24 μm data available to give complete coverage of the entire $25' \times 25'$ field centered on each cluster in the sample.

The 24 μm data were reduced and combined with the Data Analysis Tool (DAT) developed by the MIPS instrument team (Gordon et al. 2005). A few additional processing steps were also applied as described in Egami et al. (2006). The data were resampled and mosaicked with half of the original instrument pixel scale ($1''.245$) to improve the spatial resolution. The 24 μm mosaics were analyzed with SExtractor (Bertin & Arnouts 1996); following the *Spitzer* Wide-area Infra-Red Extragalactic Legacy Survey (SWIRE; Lonsdale et al. 2003), we estimated the flux of objects within an aperture of diameter $21''$, and applied an aperture correction factor of 1.29. The flux detection limits and completeness of each mosaic were determined by individually inserting 500 simulated sources for a range of fluxes and determining their detection rate and recovered fluxes, using identical extraction procedures. The sources used in the simulations were formed by extracting isolated, high signal to noise and unresolved sources from the mosaic itself. From these simulations, we estimate that the 90% completeness limits of our 24 μm mosaics are typically 400 μJy, and for individual clusters in the range 300–500 μJy, the variation due to changes in the IR background levels.

2.1.2. LoCuSS Near-IR Observations

The same 22 clusters were observed either with WFCAM (Casali et al. 2007) on the 3.8 m United Kingdom Infrared Telescope (UKIRT)[10] in 2008 March–November or with NEW-

[9] This work is based in part on observations made with the Spitzer Space Telescope, which is operated by the Jet Propulsion Laboratory, California Institute of Technology under a contract with NASA (contract 1407).
[10] UKIRT is operated by the Joint Astronomy Centre on behalf of the Science and Technology Facilities Council of the United Kingdom.

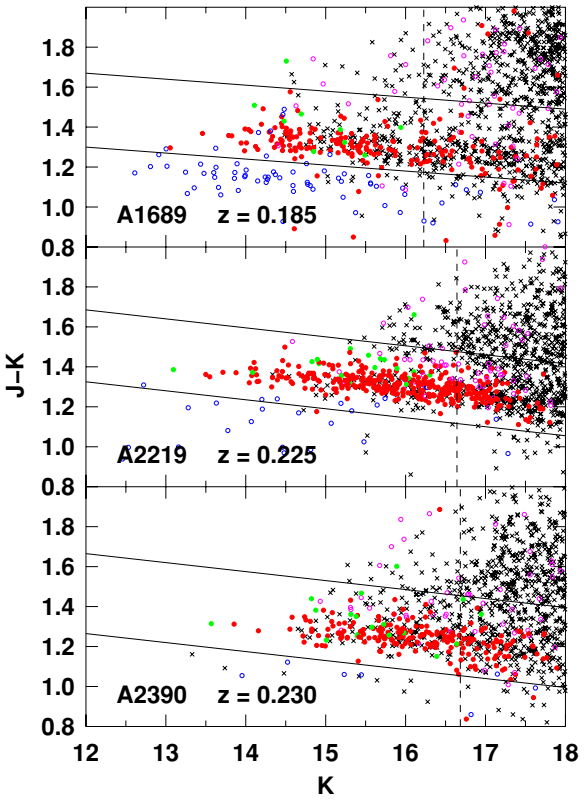

Figure 1. $J-K/K$ color–magnitude diagrams for galaxies within $1.5r_{500}$ of clusters A 1689, A 2219 and A 2390. These three clusters are shown because their spectroscopic redshift catalogs are the most complete among the 22 clusters from LoCuSS. Filled symbols indicate spectroscopically confirmed cluster members, with green (red) colors indicating those (not) having $L_{\rm IR} > 5 \times 10^{10} L_{\odot}$ based on their 24 μm fluxes. Blue and magenta open symbols indicate foreground and background galaxies with redshifts, respectively, while crosses indicate those galaxies without redshift information. The pairs of sloping lines indicate the upper and lower boundaries of the color–magnitude selection used to identify probable cluster members. The dashed line indicates our faint magnitude limit of $K^{\star}+1.5$.

(A color version of this figure is available in the online journal.)

FIRM on the 4.0 m Mayall telescope at Kitt Peak[11] on 2008 May 16–18. The WFCAM data were obtained using the same observing strategy as used by the UKIDSS Deep Extragalactic Survey (Lawrence et al. 2007), covering $52' \times 52'$ to depths of $K \sim 19$, $J \sim 21$, with exposure times of 640 s, pixel size of $0''.2$ and FWHMs $\sim 0''.8$–$1''.1$. The NEWFIRM data consist of dithered and stacked J- and K-band images with exposure times of 1800 s, and FWHM $\sim 1''.0$–$1''.5$, covering the instrument field of view $27' \times 27'$ with a $0''.4$ pixel scale. Each individual exposure was astrometrically and photometrically calibrated using 2MASS stars in the field, and stacked using IRAF, producing mosaics also reaching depths of $K \sim 19$, $J \sim 21$.

Following Haines et al. (2009), probable cluster members were identified from the JK photometry (with $J-K$ colors determined in $2''$ diameter apertures), based on the empirical observation that galaxies of a particular redshift lie along a single narrow $J-K/K$ color–magnitude relation, as shown in Figure 1 for A 1689, A 2219, and A 2390. This relation evolves redward monotonically with redshift to $z \simeq 0.5$ (see Haines et al. 2009). The NIR colors of galaxies are relatively insensitive to star formation history and dust extinction, with the $J-K$ color varying by only $\sim$0.1 mag across the entire Hubble sequence, and hence only a single sequence is seen, unlike in the optical where separate red and blue sequences are visible. This is demonstrated in Figure 1 by the 24 μm-detected cluster members (green symbols) showing the same $J-K$ colors as those cluster members not detected at 24 μm, albeit with more scatter. Indeed the 24 μm sources often lie well above the sequence, presumably reddened by dust, necessitating the use of a selection box that is asymmetric around the "red sequence" of cluster members.

The NIR color cuts are particularly efficient at removing foreground galaxies, with $> 80\%$ of $K < K^{\star}+1.5$ galaxies spectroscopically confirmed as having $z_{sp}-z_{\rm cluster} < -0.05(1+z)$ (shown by the blue open symbols in Figure 1) excluded by the lower $J-K$ color cut. However, there remains significant contamination by background galaxies in the range $z_{\rm cluster} < z \lesssim 0.5$ (open magenta symbols), driven partly by the red envelope of our color–magnitude selection function in an attempt to minimize the loss of heavily reddened cluster members (see upper sloping line in each panel of Figure 1). We correct statistically for this contamination, using galaxy counts satisfying the same color–magnitude selection in two control fields. We analyzed the UKIDSS-DXS Lockman Hole and XMM-LSS fields (Lawrence et al. 2007), based on JK photometry covering 2.1 deg^2 in total, obtained via the same observing strategy, reduction and calibration pipelines, as our WFCAM data. These fields also have publicly available 24 μm MIPS photometry from SWIRE DR2 catalogs (Lonsdale et al. 2003)[12] which are complete to 450 μJy.

With the exception of the clusters highlighted in Figure 1, the spectroscopic redshift information on galaxies in clusters from the LoCuSS sample is currently very sparse. For the purposes of this paper, we therefore define galaxies as being cluster members if they satisfy the color cuts discussed above. The fraction of star-forming galaxies in each cluster, $f_{\rm SF}$, calculated in Section 3 from these cluster galaxy catalogs is therefore net of the statistical field subtraction described above, and the error bars include a term to account for the uncertainties in this subtraction.

2.2. Low-redshift Subsample

For Coma and Abell 1367, we used archival 24 μm *Spitzer*/MIPS data covering 2×2 deg^2 in the case of Coma (PID: 83, PI G. Rieke) and $30' \times 30'$ for Abell 1367 (PID: 25, PI G. Fazio). Both data sets were obtained in the scan mode, and are complete to $\sim$330 μJy, corresponding to $L_{\rm IR} \sim 1.4 \times 10^8\, L_{\odot}$ (Bai et al. 2006). Note that the 24 μm mosaics do not extend out to the aperture of $1.5r_{500}$ adopted in this paper; we therefore estimate the 24 μm fluxes of galaxies that lie outside the observed 24 μm field of view based on their IRAS 60 μm fluxes and the empirical relation $f_{60}/f_{24} \sim 10$ (Soifer et al. 1987). The IRAS Faint Source Catalogue 60 μm completeness limit is 0.6 Jy (Beichman et al. 1988), corresponding to $L_{\rm IR} \sim 4 \times 10^{10}\, L_{\odot}$ for Coma and A 1367, or just below our $L_{\rm IR}$ selection limit used in Section 3. K-band photometry and redshifts for both of these clusters were taken from the GOLDMine[13] database (Gavazzi et al. 2003).

For the five clusters forming the core of the Shapley supercluster (A 3556, A 3558, A 3562, SC 1329-313 and SC 1327-312)

[11] Kitt Peak National Observatory, National Optical Astronomy Observatory, which is operated by the Association of Universities for Research in Astronomy (AURA) under cooperative agreement with the National Science Foundation.

[12] The SWIRE DR2 catalogs are available here: http://swire.ipac.caltech.edu/swire/astronomers/data_access.html.

[13] Available at http://goldmine.mib.infn.it/.

at $z = 0.048$, we use unpublished *Spitzer* 24 μm MIPS imaging (PID: 50510, PI: C. Haines), UKIRT/WFCAM K-band photometry and redshifts from the ACCESS survey all of which cover a $\sim 2.5 \times 1.5\,\mathrm{deg}^2$ field of view. The 24 μm mosaics are complete to $\sim$400 μJy, corresponding to $L_{\rm IR} \sim 1 \times 10^9\,L_\odot$ at the supercluster redshift. The WFCAM K-band data have exposure times 300 s, pixel scale 0.″2, and is 90% complete to $K \sim 17.5$ ($K^\star$+5.5), while our redshift coverage is $>$ 95% complete to $K^\star$+1.5. At these low redshifts, many of the 24 μm sources are resolved, and so for those galaxies with NIR diameters greater than our standard 21″ MIR aperture, we used a series of circular apertures of diameter up to 2′ (45″ for Shapley), and the optimal diameter chosen to encircle all of the galaxy's NIR flux.

2.3. Bolometric Infrared Luminosities of 24 μm Sources

The bolometric luminosity, $L_{\rm IR}$, of each 24 μm-selected cluster galaxy is estimated from its 24 μm flux using a range of infrared SEDs (Chary & Elbaz 2001; Chanial 2003; Dale et al. 2001; Lagache et al. 2003, 2004), as a function of redshift following Le Floc'h et al. (2005). We classify as star-forming those galaxies with $L_{\rm IR} > 5 \times 10^{10}\,L_\odot$, which corresponds to the 24 μm completeness limits for our five highest redshift clusters ($0.27 < z < 0.29$). Note that for all the remaining clusters at $z \simeq 0.2$, this $L_{\rm IR}$ limit lies in the range 550–1500 μJy, and hence is always well above the corresponding completeness limit of the cluster.

Assuming that the 24 μm emission is due entirely to star formation, this limit corresponds to a SFR of $\sim 8\,M_\odot\,\mathrm{yr}^{-1}$ (Kennicutt 1998). The choice of infrared SEDs introduces a spread of $L_{\rm IR}/S_{24\,\mu\rm m}$ ratios due to the range of dust temperatures assumed. This spread varies systematically with redshift, and is of the order 0.1–0.2 dex over $0 < z < 0.3$. These systematic uncertainties are incorporated into the error bars quoted in Section 3. More accurate estimates of $L_{\rm IR}$ will be possible in future with the availability of *Herschel* 100 μm and 160 μm photometry, which will allow us to fully model the reprocessed thermal emission from the dust.

Some of the 24 μm emissions could be due to dust-enshrouded active galactic nuclei (AGNs), as a significant fraction of infrared galaxies are known to be powered by a combination of AGN activity and star formation. At the typical infrared luminosities of our sample ($(0.5\text{–}2) \times 10^{11} L_\odot$), the primary power source of the 24 μm emission has been shown to be star formation in $\gtrsim$90% of the cases (e.g., Goulding & Alexander 2009). There is also a strong almost linear correlation between the 24 μm and extinction-corrected Paα fluxes over four decades in luminosity among local infrared galaxies, the latter emission shown from *Hubble Space Telescope*/Near-Infrared Camera and Multi-Object Spectrometer (*HST*/NICMOS) imaging to be in the form of nuclear star formation rings or more extended emission from spiral arms or disks (Alonso-Herrero et al. 2006).

For our low-redshift cluster galaxy sample, we can constrain the dominant power source behind the observed 24 μm emission, using both optical spectroscopy and the morphology of the 24 μm emission (extended/unresolved). For this purpose, we use SDSS DR7 (Abazajian et al. 2009) for Coma and Abell 1367 members, or Smith et al. (2007) for galaxies in the Shapley supercluster, to place 24 μm-selected galaxies on the emission-line diagnostic diagrams of Baldwin et al. (1981). We only consider it likely that an AGN as the dominant contributor to the infrared flux if a galaxy is *both* optically classified as an AGN *and* the 24 μm emission is unresolved, as Brand et al. (2009) found in a study of $0.15 < z < 0.30$ galaxies with $f_{24} > 0.3$ mJy that the bulk of those galaxies classified optically as AGNs also had infrared colors indicative of polycyclic aromatic hydrocarbon emission from star formation.

We find that all 13 infrared-luminous galaxies in Coma/A1367 have *either* extended 24 μm emission or optical emission-line ratios indicative of star formation. In Shapley supercluster, we find just three of 29 infrared-luminous galaxies are classified as AGNs.

Considering also an X-ray-bright AGN, Martini et al. (2006) studied X-ray luminous ($L_X > 10^{41}$ erg s^{-1}) AGNs in eight clusters at $0.06 < z < 0.31$, obtaining an AGN fraction of $\sim 5\%$ among $M_R < -20$ galaxies. Eastman et al. (2007) found evidence that the X-ray AGN ($L_X > 10^{42}$ erg s^{-1}) fraction increases by a factor 20 from $z = 0.2$ to $z = 0.6$. We consider what fraction of these X-ray luminous AGNs are also strong MIR emitters. For Abell 1689, which is in the Martini et al. (2006) sample, only one of our infrared-bright sources is found to be an X-ray AGN, while for Abell 1758, we find just two of our 82 24 μm detections to coincide with an X-ray point source (Haines et al. 2009).

3. RESULTS

3.1. The Mid-Infrared Butcher–Oemler Effect

For each cluster, we compute the fraction of star-forming cluster members ($f_{\rm SF}$) within $1.5r_{500}$ ($\sim 1.0r_{200}$; Sanderson & Ponman 2003), after selecting by rest-frame K-band magnitude ($M_K \leqslant M_K^\star$+1.5), and bolometric infrared luminosity ($L_{\rm IR} > 5 \times 10^{10}\,L_\odot$). We exclude the brightest cluster galaxy (BCG) from each cluster, due to their unique star formation histories (Lin & Mohr 2004) and the direct link between BCG activity and the presence of cooling flows within clusters (Edge 1991). We model the redshift evolution of $K^\star$ as a Bruzual & Charlot (2003) stellar population formed at $z = 4$ with an exponentially decaying SFR of timescale 1 Gyr, normalized to match the present day value of $M_K^\star = -24.60 \pm 0.03$ (Jones et al. 2006) for field galaxies. We note that this value is slightly brighter than those observed for galaxy clusters, e.g., $M_K^\star = -24.58 \pm 0.40$ (Balogh et al. 2001), $M_K^\star = -24.34 \pm 0.01$ (Lin et al. 2004) (for $\alpha = 1.1$), but we prefer to refer to a "global" value for M_K^*. The measurements of r_{500} for clusters at $0.15 < z < 0.3$ are obtained from analysis of *Chandra X-ray* observations, both from the archive and our own Cycle 10 observations (PID: 10800565; PI: G.P. Smith); the details of this analysis can be found in Sanderson et al. (2009). Values of r_{500} for the remaining clusters are taken from the literature (Sanderson et al. 2006).

The value of $f_{\rm SF}$ for each cluster is listed in Table 1; the quoted uncertainties include the binomial error calculated using the formulas in Gehrels (1986), and uncertainties on the statistical subtraction of field galaxies. We show $f_{\rm SF}$ versus redshift—the MIR BO effect—in Figure 2, finding a steady increase in $f_{\rm SF}$ with redshift, from $\langle f_{\rm SF}\rangle = 0.035 \pm 0.023$ at $z < 0.05$ to $\langle f_{\rm SF}\rangle = 0.053 \pm 0.027$ at $0.15 \leqslant z \leqslant 0.25$, and $\langle f_{\rm SF}\rangle = 0.085 \pm 0.038$ at $0.25 \leqslant z \leqslant 0.29$, where the quoted uncertainties are the rms scatter around the means. This trend is consistent with that found for the original BO study, whereby f_b increases from 0.053 ± 0.054 at $z < 0.08$ to 0.098 ± 0.062 over $0.17 \leqslant z \leqslant 0.28$, although we caution that given the rather diverse counting radii, cluster and galaxy selection criteria used, this may be coincidental.

To quantify the redshift evolution of $f_{\rm SF}$, we fit the following relation to the individual data points at $z < 0.3$ shown in

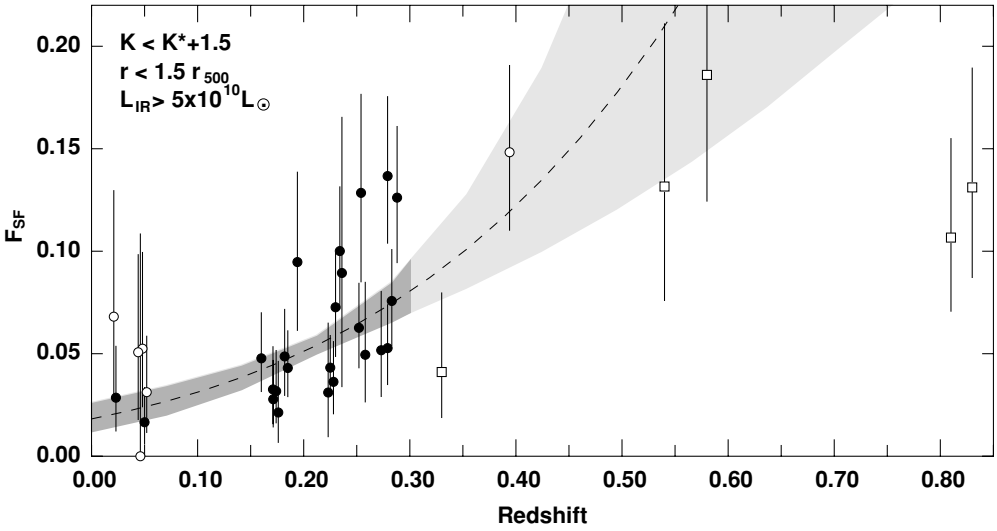

Figure 2. MIR BO effect. The estimated fraction of $M_K \leqslant M_K^\star+1.5$ cluster members within $1.5r_{500}$ having $L_{\rm IR} > 5 \times 10^{10}\,L_\odot$. The dashed line indicates the best-fitting evolutionary fit of the form $f_{\rm SF} = f_0(1+z)^n$ to the $z < 0.3$ clusters, and the shaded region indicates the 1σ confidence region to the fit, with the lighter colors showing the extrapolation of the fit beyond $z = 0.3$. Solid circles indicate clusters with $L_{\rm X} > 3 \times 10^{44}{\rm erg\,s^{-1}}$, while open circles indicate less X-ray luminous clusters. The open squares indicate the values of $f_{\rm SF}$ taken from the Saintonge et al. (2008) $z > 0.3$ sample.

Figure 2: $f_{\rm SF} = f_0(1+z)^n$. The best-fit exponent is $n = 5.7^{+2.1}_{-1.8}$; the corresponding curve and 1σ confidence interval are overplotted in Figure 2. Extrapolating the best-fit relation (shown as lighter shaded region) reveals that it is consistent with the value of $f_{\rm SF}$ that we measure for Cl 0024 at $z = 0.395$. Note that our measurement of $f_{\rm SF} = 0.15 \pm 0.04$ for this cluster is consistent with that obtained by Geach et al. (2006). The rapid rate of evolution does not depend strongly on the choice of limiting radius; repeating the calculation using galaxies selected within r_{500}, we obtain $n = 5.0^{+2.9}_{-2.3}$; however, the values of $f_{\rm SF}$ are in this case systematically lower than their counterparts within $1.5r_{500}$ by $\sim$20%.

Our use of NIR color cuts could exclude some star-forming cluster members, whose colors in Figure 1 show a much greater spread than their passive counterparts, resulting in a fraction lying outside our color limits. To test this possibility, we redo the analysis, this time without any color cuts. The overall trend and scatter are unchanged, although as the correction for field contamination increases, so do the uncertainties both in $f_{\rm SF}$ for individual clusters, and the overall measured evolutionary trend, for which we obtain $n = 6.5^{+2.5}_{-2.0}$. The slight increase in $\langle f_{\rm SF}\rangle = 0.099 \pm 0.036$ at $0.25 \leqslant z \leqslant 0.29$ obtained when we remove the color cuts, suggests that a small fraction ($\sim$ 10%) of 24 μm cluster members may be lost by our color cuts, but that this is not significant.

The measured level of redshift evolution is also consistent with the MIR BO study of eight clusters over $0.02 < z < 0.83$ by Saintonge et al. (2008) at least for their $z < 0.4$ clusters. The absence of a statistical sample of clusters at $z > 0.3$ clusters in either this study or that of Saintonge et al. (2008), makes it difficult to interpret whether the strong redshift evolution might extend to higher redshift. However, their two clusters at $z \simeq 0.8$ (shown as open squares in Figure 2) are inconsistent with an extrapolation of our best-fit evolutionary model at 2σ. This suggests that the MIR BO effect might saturate beyond $z \sim 0.5$, although we note that they use a smaller fixed 1 Mpc counting radius to estimate their $f_{\rm SF}$.

A possible caveat to this analysis is that our $L_{\rm IR}$ threshold for selecting star-forming galaxies lies within the exponential region of the infrared luminosity function (LF), particularly at $z \sim 0$ (Bai et al. 2006 estimate $L_{\rm IR}^\star = 3 \times 10^{10} L_\odot$ for Coma) so that small changes in the threshold could produce large changes in $f_{\rm SF}$. We are sensitive here to only the most actively star-forming galaxies, missing a significant fraction of the population of normal star-forming galaxies, which are known to form a well-defined sequence in the specific SFR/stellar mass plane (Noeske et al. 2007). As a result, we might expect our values of $f_{\rm SF}$ to be systematically below the f_b values obtained for the same clusters. However, when averaging over the six clusters in common with Smail et al. (1998), we find no significant difference between our $f_{\rm SF}$ values and their f_b values. We also note that only two of the low-redshift clusters (Coma and A 3558) have X-ray luminosities comparable with the clusters from LoCuSS at $0.15 \leqslant z \leqslant 0.3$. Strictly speaking, this analysis therefore does not compare like with like at low and intermediate redshifts. However, the results in this and subsequent sections are robust to the exclusion of all clusters at $z < 0.1$ except for Coma and A 3358, in which case we now obtain $f_{\rm SF} = 7.8^{+2.3}_{-2.3}$ within $1.5\,r_{500}$. Indeed the primary driver of our observed rapid evolution in $f_{\rm SF}$ is that produced *within* the LoCuSS sample, rather than the comparison to the low-redshift subsample. This mismatch is therefore not a major concern; however, it is unfortunate that there does not exist a suitable comparable set of panoramic MIR observations of rich clusters at $z < 0.1$.

3.2. MIR BO Effect and the Global Decline in Star Formation

We now investigate whether the redshift evolution of $f_{\rm SF}$ is caused by physical processes operating within clusters, or simply reflects the global decline in star formation since $z \sim 1$, or a combination of both. The redshift evolution of $f_{\rm SF}$ discussed above is stronger than that of the global SFR. For example, Zheng et al. (2007) showed that the specific UV+IR-determined SFR has declined by a factor $\sim$10 since $z \sim 1$, independent of galaxy mass, while the specific SFRs of local galaxies are $\sim$0.3 dex lower than those of $0.2 < z < 0.4$ galaxies of the same mass. Le Floc'h et al. (2005) find strong evolution in the global infrared LF since $z \sim 1$, characterized by $L_{\rm IR}^\star \propto (1+z)^m$ with

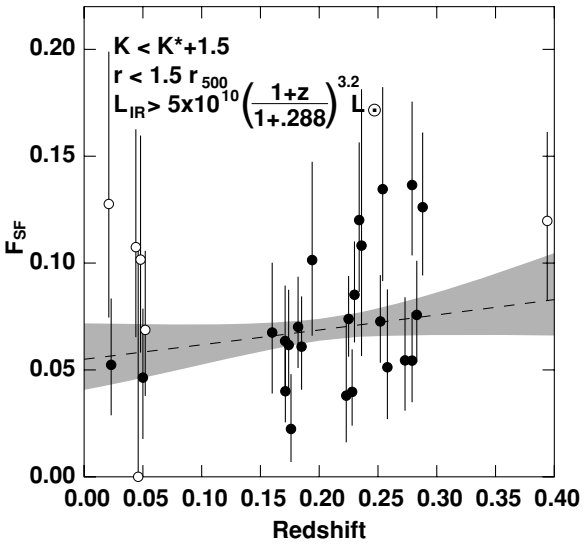

Figure 3. As in Figure 2, but taking into account the evolution of the MIR luminosity function of field galaxies, $L^{\star}_{\rm IR} \propto (1+z)^{3.2}$, when identifying galaxies as star forming. Symbols are as in Figure 2.

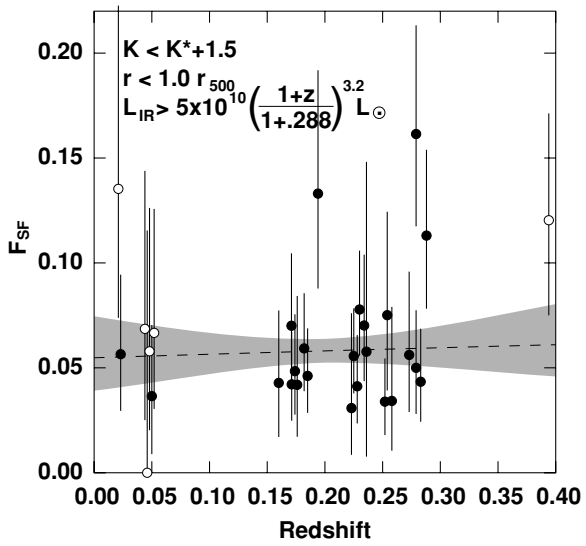

Figure 4. As in Figure 3, but considering only those galaxies within r_{500}. Symbols are as in Figure 2.

$m = 3.2^{+0.7}_{-0.2}$, similar to the $m = 3.0 \pm 0.3$ obtained by Pérez-González et al. (2005). Noeske et al. (2007) also find that the median SFR at a fixed stellar mass of the *entire* sequence of star-forming galaxies shifts downward by a factor of 3 from $z = 0.98$ to $z = 0.36$, corresponding to an evolution of SFR$\propto(1+z)^{2.9}$.

Studies of the MIR LFs of nearby clusters find the shape and $L^{*}_{\rm IR}$ to be consistent with those of field galaxies, while the evolution with redshift to $z \simeq 0.8$ of $L^{*}_{\rm IR} \propto (1+z)^{3.2\pm0.7}$ is also indistinguishable from the field (Bai et al. 2009). Similarly, Finn et al. (2008) find that the Hα luminosities of individual cluster galaxies have declined by a factor of up to $\sim$10, since $z \sim 0.75$, comparable to that of field galaxies over a similar redshift interval.

To quantify the excess evolution of $f_{\rm SF}$ over the global evolution of star formation, we therefore repeat the analysis in Section 3.1, this time allowing the luminosity threshold above which galaxies are counted in the numerator of $f_{\rm SF}$ to scale with redshift as follows: $L_{\rm IR} > 5 \times 10^{10}[(1+z)/(1+z_{\rm max})]^{k}$, with $k = 3.2$ chosen to be representative of the results discussed above, and $z_{\rm max} = 0.288$, corresponding to the highest cluster redshift to which we fit the redshift evolution model. This is analogous to the use of differential k-corrections to identify "blue" galaxies with the same spectral classes of galaxies at all redshifts (e.g., Andreon et al. 2006; Loh et al. 2008) rather than the fixed $\Delta_{B-V} = 0.2$ criterion of BO84. We replot the MIR BO effect using this selection function in Figure 3, and find (as expected) that the redshift evolution has largely disappeared: $f_{\rm SF} = 0.072 \pm 0.044$ for the seven clusters at $z < 0.1$, and $f_{\rm SF} = 0.074 \pm 0.033$ for the 22 clusters at $0.15 < z < 0.3$. Again, we fit a model to the data of the form $f_{\rm SF}(z) \propto (1+z)^{n}$, obtaining $n = 1.22^{+1.52}_{-1.38}$, as shown by the dashed curve and error envelope in Figure 3.

This level of evolution is consistent with the expected increase in the fraction of galaxies accreted by massive clusters within the previous Gyr. Berrier et al. (2009) show that although the accretion rate of galaxies into massive clusters has remained constant since $z \sim 1$, half of the cluster galaxy population has been accreted since $z \sim 0.4$, and so the *fraction* of recently accreted galaxies should appear to double from $z \sim 0$ to $z \sim 0.4$. This suggests that the "residual" redshift evolution seen in Figure 3, albeit at modest statistical significance, is attributable to the fate of galaxies after they have fallen into clusters. Galaxy populations that have recently fallen into clusters are most easily identified in photometric observational data at large cluster-centric radii, thus overcoming the projection of the three-dimensional distribution of galaxies onto the sky. To gain a rough idea of the location of the galaxies responsible for the redshift evolution seen in Figure 3, we modify further the selection function, this time restricting the range of cluster-centric radii to $< r_{500}$, again using the "differential k-correction" approach to $L_{\rm IR}$ selection. The results of this modified selection are shown in Figure 4, with the best-fit redshift evolution model again shown as the dashed curve; the best-fit model has $n = 0.32^{+1.74}_{-1.66}$. We also fit a model with just a single parameter—a redshift-invariant value of $f_{\rm SF}$—obtaining $f_{\rm SF} = 0.056 \pm 0.004$, with a reduced chi-squared value of 0.72, confirming that the scatter of the data around this value can be explained simply by the observational uncertainties, without recourse to either intrinsic cluster-to-cluster scatter or redshift evolution.

In summary, these results are consistent with the global decline in IR activity in field galaxies since $z = 1$. As field galaxies fall into clusters some of them suffer an increase in IR activity at $> r_{500}$, presumably due to star formation induced by gentle processes in their local environment at large radii. The amplitude of this increase, as measured via $f_{\rm SF}$, evolves with redshift at a rate which is not significantly different from zero, but nonetheless consistent with the fractional rate at which galaxies are accreted into rich clusters. Nevertheless, there is still significant cluster-to-cluster scatter, and so now we turn to whether this variation in $f_{\rm SF}$ might be due to some global property of the cluster.

3.3. Correlations with Cluster Properties

A number of previous studies (e.g., Wake et al. 2005; Popesso et al. 2007; Aguerri et al. 2007) have looked for correlations between the X-ray luminosity of clusters and the fraction of star-forming galaxies (or equivalently blue/emission line), with the aim of ascertaining if ram pressure stripping and/or starvation could be the dominant mechanisms for quenching star formation in infalling galaxies, and driving the observed SF–density relation.

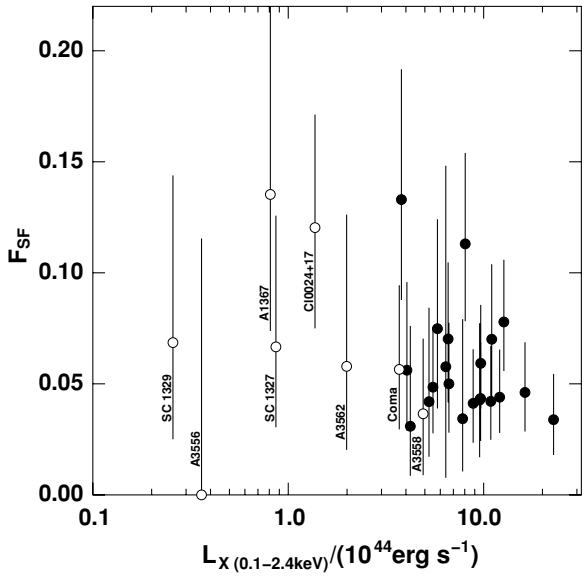

Figure 5. Relation between the fraction of star-forming cluster galaxies within r_{500} and the X-ray luminosity. Solid symbols indicate LoCuSS clusters, while labeled open symbols indicate the non-LoCuSS subsample.

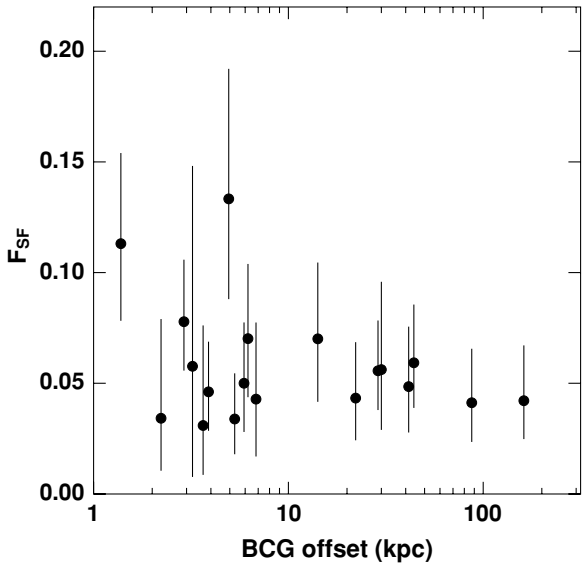

Figure 6. Relation between the fraction of star-forming cluster galaxies within r_{500} and the offset of the brightest cluster galaxy from the peak of X-ray emission.

In Figure 5, we plot the fraction of star-forming cluster galaxies within r_{500} against the cluster X-ray luminosity in the 0.1–2.4 keV band taken directly from the *ROSAT* All Sky Survey cluster catalogs (Ebeling et al. 1998, 2000; Böhringer et al. 2004), using the same evolving L_{IR} cut as described in Section 3.2. We exclude here Abell 689 as its X-ray luminosity is dominated by a BL Lac. As previously mentioned, clusters in the LoCuSS sample are more X-ray luminous ($L_X > 2 \times 10^{44} \mathrm{erg\,s^{-1}}$) than all of the other clusters except Coma and A 3558. Overall there is no apparent trend of f_{SF} with X-ray luminosity, in agreement with Wake et al. (2005), which might seem to rule out ICM-related processes. However, this may simply be a saturation effect, in that ram pressure stripping is effective at stripping the gas in all infalling galaxies even for the lowest X-ray luminosity clusters ($L_X \sim 3 \times 10^{43} \mathrm{erg\,s^{-1}}$) in our sample. Indeed, Poggianti et al. (2006) find a strong anti-correlation between the fraction of emission-line galaxies and cluster velocity dispersion for $\sigma \lesssim 550\,\mathrm{km\,s^{-1}}$, but for richer systems there are no systematic trends. This may also explain the observed negative trend between f_b and L_X seen by Popesso et al. (2007), as their cluster sample extends to much poorer systems than ours or that of Wake et al. (2005).

As discussed in Section 1, it has been suggested that the level of star formation activity in a galaxy cluster correlates with its dynamical status, with merging clusters showing increased activity with respect to their undisturbed counterparts (Miller & Owen 2003; Miller et al. 2005; Metcalfe et al. 2005). No single measure exists in the literature that unambiguously identifies a cluster as being "disturbed," i.e., undergoing a merger. Nevertheless, several measures do appear to correlate with cluster dynamical status, such as the presence or absence of a cool core in the X-ray temperature profile, the cuspiness of the density profile, or the offset of the BCG from the peak of X-ray emission (e.g., Smith et al. 2005b). In these cases, merging clusters are typically identified with non-cool core clusters with flatter density profiles, and BCGs with large offsets from the X-ray peak.

In Figure 6, we therefore plot the fraction of star-forming galaxies within r_{500} versus the projected physical distance between the BCG and the peak of X-ray emission, for the LoCuSS subsample, the latter measurement being taken from Sanderson et al. (2009). Interestingly, there is no obvious correlation between the BCG offset and f_{SF}, or alternatively when comparing the cuspiness of the cluster density profiles with f_{SF}. We also obtain similar results when considering galaxies within $1.5\,r_{500}$. Among the LoCuSS sample, neither Abell 1758 or Abell 1914, which are known merging clusters (Okabe & Umetsu 2008), have high f_{SF}'s, while Abell 611 which appears to be a regular, relaxed cluster is among the few "active" clusters with $f_{SF} = 0.135$. Indeed, the most prominent feature in Figure 6 is the absence of clusters in the upper right quadrant of the plot, i.e., with large values of f_{SF} and large offset between BCG and X-ray peak. On the face of it, this is counter to the qualitative expectation that merging clusters contain more numerous star-forming galaxies than non-merging clusters, as suggested from the radio observations of merging clusters (not among our sample) by Miller & Owen (2003). This may suggest that at least within r_{500} many of the galaxies have already been stripped of their gas when they were accreted into the progenitor (presumably already massive) clusters, and so are unable to undergo any starburst phase triggered by the cluster merger.

3.4. Radial Population Gradients and the Infall Model

A comparison of Figures 3 and 4 indicates that for many of the clusters, the fraction of MIR sources is lower within r_{500} than $1.5r_{500}$, in some cases by a factor 2. This is suggestive of the well-known morphology density and SF versus density gradients seen in clusters, both at low and high redshifts (e.g., Dressler et al. 1997; Balogh et al. 2000; Ellingson et al. 2001; Treu et al. 2003; Smith et al. 2005a; Haines et al. 2007). It has also been noted that the blue galaxy fraction in clusters depends strongly on the radius within which the measurement is made, with f_b systematically increasing with cluster-centric radius (e.g., Ellingson et al. 2001; Wake et al. 2005).

In Figure 7 we show the composite radial gradients in the fraction of MIR luminous galaxies (as defined in Section 3.2) for clusters in three redshift bins: the seven $z \leqslant 0.05$ clusters (red squares and dashed-lines); the low-redshift half of the LoCuSS

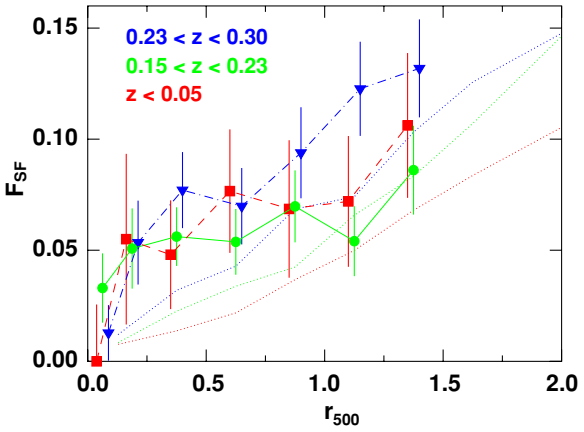

Figure 7. Composite radial gradients in the star-forming component for clusters with $z \leqslant 0.05$ (red squares and dashed lines), $0.15 < z < 0.23$ (green circles and solid lines) and $0.23 < z < 0.30$ (blue triangles and dot-dashed lines). For comparison, the dotted lines indicate the fraction of cluster members identified as infalling from the Millennium Simulation, scaled to match the corresponding field $f_{\rm SF}$ values at large radii.

(A color version of this figure is available in the online journal.)

sample ($0.15 < z < 0.23$; green circles and solid lines); and the high-redshift half of the LoCuSS sample ($0.23 < z < 0.30$; blue triangles and dot-dashed lines). The error bars indicate the uncertainty in the mean value of $f_{\rm SF}$ for each sub-sample in each bin and not the cluster-to-cluster scatter. Each redshift bin shows a clear increase in $f_{\rm SF}$ with projected cluster-centric radius, although within the uncertainties we find no strong evidence for redshift evolution in the radial trends plotted in Figure 7. However, outside r_{500}, there appears to be a modest excess of galaxies in the highest redshift subsample. This could be due to an increase in the fractional accretion rate of infalling galaxies with redshift, and/or an increase in the level of *triggered/enhanced* star formation in galaxies as they encounter the cluster environment for the first time, such as observed by Moran et al. (2005) for galaxies at the virial radius of Cl 0024+16. Similarly, Gallazzi et al. (2009) find a significant population of galaxies undergoing highly obscured star formation, preferentially located in intermediate-density environments typical of those found near the cluster virial radius, while Fadda et al. (2008) find enhanced star formation activity at $r > r_{500}$ along two filaments feeding Abell 1763. These trends are also qualitatively consistent with Ellingson et al. (2001), who found a steepening in the population gradients in clusters at $0.30 < z < 0.55$ relative to those at $0.18 < z < 0.30$, and can explain the difference in the levels of evolution seen in Figures 3 and 4.

To test our infall interpretation of the radial trends seen in Figures 3, 4, and 7, we examined galaxies falling into 20 massive clusters ($M_{\rm vir} > 10^{15}\,M_{\odot}$) from the Millennium Simulation (Springel et al. 2005). These simulations cover a $(500h^{-1}{\rm Mpc})^3$ volume, producing DM halo and galaxy catalogs based on the semianalytic models (GALFORM) of Bower et al. (2006) for which positions, peculiar velocities, absolute magnitudes and halo masses are all provided at 63 snapshots to $z = 0$, allowing the orbit of each galaxy with respect to the cluster center to be followed. We select member galaxies from these 20 clusters that have $K < K^{\star}+1.5$, and lie within 5 Mpc of the cluster center, and identify which ones are infalling into the cluster for the first time. The fraction of infalling galaxies increases approximately *linearly* with projected radius from close to zero at the cluster center to ∼25% at r_{500} and ∼ 55% at $2\,r_{500}$ until we reach $\sim 4\,r_{500}$, beyond which we would not expect to find any galaxies that have passed once through the cluster (Mamon et al. 2004). We find no redshift dependence for $f_{\rm infalling}(r/r_{500})$ within the simulations, at least over the redshift interval $0 < z < 0.3$.

We then consider a simple toy model in which the star formation in these infalling galaxies is instantaneously quenched once they pass through the cluster core. We should not expect that all infalling galaxies are star forming, a significant fraction will already be passive either due to pre-processing within groups or through internal mechanisms such as an AGN feedback. We therefore use the galaxies from the UKIDSS-DXS fields in Section 2.1 to estimate the fraction of galaxies in the field that would satisfy our selection criteria, obtaining $f_{\rm SF} = 0.25 \pm 0.03$ for the $0.15 < z < 0.23$ clusters and $f_{\rm SF} = 0.29 \pm 0.04$ for the $0.23 < z < 0.30$ clusters, and use these values to re-normalize the radial profile of the Millennium galaxies at $4\,r_{500}$. For the low-redshift bin, we measure $f_{\rm SF}$ from the 561 $M_K < M_K^* + 1.5$ galaxies (taken from the NYU-VAGC; Blanton et al. 2005) from the SDSS DR7 having redshifts $z < 0.1$ also having 24 μm photometry from SWIRE, obtaining $f_{\rm SF} = 0.19 \pm 0.02$. Note that we are not using the GALFORM-produced SFRs to identify star-forming galaxies, the only model-based parameter we consider is the K-band luminosity.

The re-normalized curves are overplotted on Figure 7 as dotted lines whose color corresponds to its redshift bin. These show the same general trend for $f_{\rm SF}$ to increase monotonically with cluster-centric radius. This consistency supports our interpretation of the radial trends in the data as arising primarily from the infall of star-forming galaxies from the field and suggests that a simple scenario where infalling star-forming galaxies are quenched once they pass through the cluster for the first time (for example via ram pressure stripping) is valid at least as a first-order approximation to model the evolution of the cluster galaxy population. The main caveat to this picture is that the observed trends in $f_{\rm SF}$ appear to lie systematically above the predictions from the simple infall model for all redshift bins over $0.25 < (r/r_{500}) < 1.5$. One possible cause is projection effects, which can produce dramatic increases in the $f_{\rm SF}$ for *individual* clusters due to the presence of line-of-sight filaments and groups associated with the large-scale structure in which the cluster is embedded, at physical distances 5–20 Mpc from the cluster, and which are not included in our simple infall model. Alternatively, this excess may indicate star formation *triggered* by environmental processes, or a rather more gradual reduction in star formation than the instantaneous shutdown in star formation modeled here. Note that in our model, we make no distinction between those galaxies which pass through the cluster core on almost radial orbits, and those which travel on more circular orbits, never passing within $0.5\,r_{500}$. In future papers, we will use the spectroscopic redshift information that is becoming available from our MMT/Hectospec redshift survey to examine in detail the properties and evolution of the MIR-bright and UV-bright cluster galaxy populations within the context of the infall scenario.

4. SUMMARY AND CONCLUSIONS

We have presented a study of the MIR properties of galaxies in a representative sample of 30 massive galaxy clusters over the redshift range $0 < z < 0.4$, taking advantage of panoramic *Spitzer*/MIPS 24 μm and ground-based NIR observations from the LoCuSS and ACCESS surveys. We revisited the Butcher–Oemler effect, using our infrared data both to reduce

uncertainties on photometric selection of likely cluster members and to overcome the strong dust obscuration (∼10–30×) previously identified in comparative optical/infrared studies. We mainly considered f_{SF}, the fraction of massive cluster galaxies ($K < K^{\star}+1.5$) within $1.5\,r_{500}$ with $L_{IR} > 5 \times 10^{10}\,L_{\odot}$. We find that $\langle f_{SF} \rangle$ increases steadily with redshift from 0.035 ± 0.023 at $z < 0.05$ to 0.053 ± 0.027 at $0.15 \leqslant z \leqslant 0.25$, and 0.085 ± 0.038 at $0.25 \leqslant z \leqslant 0.29$, where the quoted uncertainties are the rms scatter around the means. This trend is consistent with the trends in f_b found by previous optical studies (e.g., Smail et al. 1998; Aguerri et al. 2007); however, the clusters-to-cluster scatter in f_{SF} at fixed redshift is roughly half of that seen in f_b. The lower scatter in our results is likely due to a combination of our use of NIR data to select likely cluster galaxies and the different physics probed by optical and IR data.

We fit a redshift evolution model of the form $f_{SF} \propto (1+z)^n$ to the observational data, obtaining a best-fit value of $n = 5.7^{+2.1}_{-1.8}$. This level of evolution exceeds that of $L^{\star}_{IR}$ in both clusters and the field (e.g., Bai et al. 2009). We therefore repeated our analysis taking into account the cosmic decline in star formation by modifying our selection function; thus, $L_{IR} > 5 \times 10^{10}[(1+z)/(1+z_{max})]^k$, with $k = 3.2$ chosen to be representative of the results such as those of Le Floc'h et al. (2005) and Zheng et al. (2007), and $z_{max} = 0.288$, corresponding to the highest cluster redshift to which we fit the redshift evolution model. The best-fit redshift evolution for this modified selection is $n = 1.22^{+1.52}_{-1.38}$. Indeed, if we restrict the galaxy samples to the central region of each cluster ($r < r_{500}$) then the fraction of cluster galaxies identified as star forming from their MIR emission remains constant at ∼5% over $0 < z < 0.4$. This suggests that redshift evolution of f_{SF} can be interpreted as a consequence primarily of the rapid evolution in the SFRs of *field* galaxies over this period, which are accreted onto the clusters at a constant rate, before being quenched by cluster-related processes. However, the small residual redshift evolution seen at $r > r_{500}$ after removing the global decline in star formation suggests that some new star formation is triggered in clusters at large radii, presumably due to gentle processes at play in the local group environments within which galaxies arrive in the clusters.

Globally, there is therefore little evolution in the cluster population itself, as the infall rate of field galaxies is expected to remain constant out to $z \sim 1$ (Berrier et al. 2009), while the efficiency of the processes which quench star formation in the recently accreted galaxies (e.g., ram pressure stripping) should not evolve rapidly. This lack of evolution in the cluster galaxy population to $z \sim 0.5$ and beyond is consistent with recent studies looking at the BO effect (Smail et al. 1998; De Propris et al. 2003; Homeier et al. 2005; Wake et al. 2005; Andreon et al. 2006) and the morphology–density relation (Holden et al. 2007). All of these studies indicate that much of the apparent evolution in earlier optical BO studies was due to the use of optical luminosities to select galaxies, such that the trends were due to low-mass galaxies undergoing starbursts in the higher redshift samples (see Figure 2 of Holden et al. 2007), or biases resulting from the cluster sample itself.

The view that the bulk of star formation in clusters simply represents recently accreted field galaxies is consistent with the observed constancy of the shape of the UV and IR LFs (both $L^{\star}$ and α) from clusters to the field in the local universe (Cortese et al. 2005; Bai et al. 2006), while Mercurio et al. (2006) find no variation in the optical LF of blue (i.e., star-forming) galaxies with environment. Moreover, the cluster IR and Hα LFs have been shown to evolve in the same manner as field LFs, declining by a factor ∼10 since $z \sim 1$ (Bai et al. 2009; Finn et al. 2008).

We have investigated the effects of cluster properties on the level of star formation in their member galaxies, finding no apparent dependence of f_{SF} on either X-ray luminosity or on the dynamical status of the cluster. The absence of correlation with L_X may seem to rule out ICM-related processes as the main route by which star formation is quenched in dense environments, but this may simply be a saturation effect, in that ram pressure stripping is effective in stripping the gas in all infalling galaxies even for the lowest X-ray luminosity clusters in our sample. Studies which examine much poorer systems find strong anti-correlations between f_{SF} and L_X or σ_v, which then flatten off for the $\sigma > 550$ km s^{-1} systems comparable to those which make up our sample. The lack of correlation between f_{SF} and the dynamical status of the clusters is surprising and seems to contradict previous studies (e.g., Miller & Owen 2003). This may suggest that at least within r_{500}, galaxies have already been stripped of their gas, and so are unable to undergo any starburst phase triggered by the cluster merger. However, at larger radii there may still be enhanced activity during certain phases of cluster mergers, as the infalling galaxies should still be gas-rich. Expanding on this, composite population gradients show a smooth increase in the fraction of star-forming galaxies from close to zero in the cluster cores to 7%–13% by $2r_{500}$. Through comparison with numerical simulations, we find that these gradual trends are consistent with a simple model in which the star-forming galaxies are infalling into the cluster for the first time (usually on highly radial orbits), and then quenched somehow once they pass through the cluster core, for example via ram pressure stripping. Within r_{500} there is no apparent evolution in the radial population gradients, but beyond r_{500} we find a possible excess of 24 μm-bright galaxies in the highest redshift bin ($0.23 < z < 0.30$), suggestive of either enhanced star formation in the cluster infall regions similar to that found by Moran et al. (2005), Gallazzi et al. (2009), or Fadda et al. (2008), or an increase in the fraction of infalling galaxies, comparable to that expected from simulations (Berrier et al. 2009).

In the future, we will further develop these results using spectroscopic redshifts for the cluster galaxy populations from our ongoing MMT/Hectospec survey, plus weak-lensing (Okabe et al. 2009) and X-ray (Zhang et al. 2008) data to investigate in detail the relationship between the star-forming galaxy populations in clusters and the dynamical state of the host clusters.

C.P.H., G.P.S., A.J.R.S., and R.J.S. acknowledge financial support from STFC. G.P.S. and R.S.E. acknowledge support from the Royal Society. This work was partly carried out within the FP7-PEOPLE-IRSES-2008 project ACCESS. We acknowledge NASA funding for this project under the Spitzer program GO:40872. C.P.H. and G.P.S. thank Trevor Ponman and Alastair Edge for helpful comments on early drafts of this article. We thank our colleagues in the LoCuSS collaboration for their encouragement and help. We also thank the Virgo Consortium for making the Millennium Simulation available to the community.

REFERENCES

Abazajian, K. N., et al. 2009, ApJS, 182, 543
Aguerri, J. A. L., Sánchez-Janssen, R., & Muñoz-Tuñón, 2007, A&A, 471, 17
Alonso-Herrero, A., Rieke, G. H., Rieke, M. J., Colina, L., Pérez-González, P. G., & Ryder, S. D. 2006, ApJ, 650, 835
Andreon, S., & Ettori, S. 1999, ApJ, 516, 647

Andreon, S., Quintana, H., Tajer, M., Galaz, G., & Surdej, J. 2006, MNRAS, 365, 915
Bai, L., Rieke, G. H., Rieke, M. J., Christlein, D., & Zabludoff, A. 2009, ApJ, 693, 1840
Bai, L., Rieke, G. H., Rieke, M. J., Hinz, J. L., Kelly, D. M., & Blaylock, M. 2006, ApJ, 639, 827
Baldwin, J. A., Phillips, M. M., & Terlevich, R. 1981, PASP, 93, 5
Balogh, M. L., Christlein, D., Zabludoff, A. I., & Zaritsky, D. 2001, ApJ, 557, 117
Balogh, M. L., Navarro, J. F., & Morris, S. L. 2000, ApJ, 540, 113
Beichman, C. A., Neugebauer, G., Habing, H. J., Clegg, P. E., & Chester (ed.), T. J. 1988, Infrared Astronomical Satellite (IRAS) Catalogues and Atlases 1, Explanatory Supplement (Washington, DC: NASA)
Berrier, J. C., Stewart, K. R., Bullock, J. S., Purcell, C. W., & Barton, E. J. 2009, ApJ, 690, 1292
Bertin, E., & Arnouts, S. 1996, A&AS, 117, 393
Biviano, A., et al. 2004, A&A, 425, 33
Blanton, M., et al. 2005, AJ, 129, 2562
Böhringer, H., et al. 2004, A&A, 425, 367
Boselli, A., & Gavazzi, G. 2006, PASP, 118, 517
Bower, R. G., et al. 2006, MNRAS, 370, 645
Brand, K., et al. 2009, ApJ, 693, 340
Bruzual, G., & Charlot, S. 2003, MNRAS, 344, 1000
Butcher, H., & Oemler, A., Jr. 1978, ApJ, 219, 18
Butcher, H., & Oemler, A., Jr. 1984, ApJ, 284, 426
Calzetti, D., et al. 2007, ApJ, 666, 870
Casali, M., et al. 2007, A&A, 467, 777
Chanial, P. 2003, PhD thesis, Univ. of Paris
Chary, R., & Elbaz, D. 2001, ApJ, 556, 562
Cortese, L., et al. 2005, ApJ, 623, L17
Dale, D. A., Helou, G., Contursi, A., Silbermann, N. A., & Kolhatkar, S. 2001, ApJ, 549, 215
De Propris, R., Stanford, S. A., Eisenhardt, P. R., & Dickinson, M. 2003, ApJ, 598, 20
De Propris, R., Stanford, S. A., Eisenhardt, P. R., Holden, B. P., & Rosati, P. 2007, AJ, 133, 2209
Desai, V. 2007, ApJ, 660, 1151
Dressler, A., Rigby, J., Oemler, A., Jr., Fritz, J., Poggianti, B., Rieke, G., & Bai, L. 2009, ApJ, 693, 140
Dressler, A., et al. 1997, ApJ, 490, 577
Duc, P.-A., et al. 2002, A&A, 382, 60
Eastman, J., Martini, P., Sivakoff, G., Kelson, D. D., Mulchaey, J. S., & Tran, K.-V. 2007, ApJ, 664, L9
Ebeling, H., Edge, A. C., Allen, S. W., Crawford, C. S., Fabian, A. C., & Huchra, J. P. 2000, MNRAS, 318, 333
Ebeling, H., Edge, A. C., Bohringer, H., Allen, S. W., Crawford, C. S., Fabian, A. C., Voges, W., & Huchra, J. P. 1998, MNRAS, 301, 881
Edge, A. C. 1991, MNRAS, 250, 103
Ellingson, E., Lin, H., Yee, H. K. C., & Carlberg, R. G. 2001, ApJ, 547, 609
Egami, E., et al. 2006, ApJ, 647, 922
Fadda, D., Biviano, A., Marleau, F. R., Storrie-Lombardi, L. J., & Durret, F. 2008, ApJ, 672, L9
Fadda, D., Elbaz, D., Duc, P.-A., Flores, H., Franceschini, A., Cesarsky, C. J., & Moor wood, A. F. M. 2000, A&A, 361, 827
Fairley, B. W., Jones, L. R., Wake, D. A., Collins, C. A., Burke, D. J., Nichol, R. C., & Romer, A. K. 2002, MNRAS, 330, 755
Farrah, D., et al. 2007, ApJ, 667, 149
Finn, R. A., Balogh, M. L., Zaritsky, D., Miller, C. J., & Nichol, R. C. 2008, ApJ, 679, 279
Gallazzi, A., et al. 2009, ApJ, 690, 1883
Gavazzi, G., et al. 2003, A&A, 400, 451
Geach, J. E., Smail, I., Moran, S. M., Treu, T., & Ellis, R. S. 2009, ApJ, 691, 783
Geach, J. E., et al. 2006, ApJ, 649, 661
Gehrels, N. 1986, ApJ, 303, 336
Gordon, K. D., et al. 2005, PASP, 117, 505
Goto, T., et al. 2003, PASJ, 55, 739
Goulding, A. D., & Alexander, D. M. 2009, arXiv:0906.0772
Haines, C. P., Gargiulo, A., La Barbera, F., Mercurio, A., Merluzzi, P., & Busarello, G. 2007, MNRAS, 381, 7
Haines, C. P., Gargiulo, A., & Merluzzi, P. 2008, MNRAS, 385, 1201
Haines, C. P., et al. 2009, MNRAS, 396, 1297
Holden, B. P., et al. 2007, ApJ, 670, 190
Homeier, N. L., et al. 2005, ApJ, 626, 651
Jones, D. H., Peterson, B. A., Colless, M., & Saunders, W. 2006, MNRAS, 369, 25
Kennicutt, R. C., Jr. 1998, ARA&A, 36, 189
Kennicutt, R. C., Jr., et al. 2007, ApJ, 671, 333
Lagache, G., Dole, H., & Puget, J.-L. 2003, MNRAS, 335, 555
Lagache, G., et al. 2004, ApJS, 154, 112
Lawrence, A., et al. 2007, MNRAS, 379, 1599
Le Floc'h, E., et al. 2005, ApJ, 632, 169
Lin, Y.-T., & Mohr, J. J. 2004, ApJ, 617, 879
Lin, Y.-T., Mohr, J. J., & Stanford, S. A. 2004, ApJ, 610, 745
Loh, Y.-S., et al. 2008, ApJ, 680, 214
Lonsdale, C., et al. 2003, PASP, 115, 897
Mamon, G. A., Sanchis, T., Salvador-Solé, E., & Solanes, J. M. 2004, A&A, 414, 445
Marcillac, D., Rigby, J. R., Rieke, G. H., & Kelly, D. M. 2007, ApJ, 654, 825
Margoniner, V. E., & de Carvalho, R. R. 2000, AJ, 119, 1562
Margoniner, V. E., de Carvalho, R. R., Gal, R. R., & Djorgovski, S. G. 2001, ApJ, 548, L143
Marrone, D., et al. 2009, ApJ, 701, L114
Martini, P., Kelson, D. D., Kim, E., Mulchaey, J. S., & Alex, A. 2006, ApJ, 644, 116
Mercurio, A., et al. 2006, MNRAS, 368, 109
Metcalfe, L., Fadda, D., & Biviano, A. 2005, Space Sci. Rev., 119, 425
Miller, N. A., Oegerle, W. R., & Hill, J. M. 2005, AJ, 131, 2426
Miller, N. A., & Owen, F. N. 2003, AJ, 125, 2427
Moran, S. M., et al. 2005, ApJ, 634, 977
Moran, S. M., et al. 2007, ApJ, 671, 1503
Newberry, M. V., Kirshner, R. P., & Boroson, T. A. 1988, ApJ, 335, 629
Noeske, K. G., et al. 2007, ApJ, 660, L43
Okabe, N., Takada, M., Umetsu, K., Futamase, T., & Smith, G. P. 2009, PASJ, submitted, arXiv:0903.1103
Okabe, N., & Umetsu, K. 2008, PASJ, 60, 345
Pérez-González, P. G., et al. 2005, ApJ, 630, 82
Poggianti, B. M., et al. 2006, ApJ, 642, 188
Popesso, P., Biviano, A., Romaniello, M., & Böhringer, H. 2007, A&A, 461, 411
Postman, M., et al. 2005, ApJ, 623, 721
Rieke, G. H., et al. 2004, ApJS, 154, 25
Saintonge, A., Tran, K.-V. H., & Holden, B. P. 2008, ApJ, 685, L113
Sanderson, A. J. R., Edge, A. C., & Smith, G. P. 2009, arXiv:0906.1808
Sanderson, A. J. R., & Ponman, T. J. 2003, MNRAS, 345, 1241
Sanderson, A. J. R., Ponman, T. J., & O'Sullivan, E. 2006, MNRAS, 372, 1496
Smail, I., Edge, A. C., Ellis, R. S., & Blandford, R. D. 1998, MNRAS, 293, 124
Smith, G. P., Kneib, J.-P., Smail, I., Mazzotta, P., Ebeling, H., & Czoske, O. 2005b, MNRAS, 359, 417
Smith, G. P., & Taylor, J. E. 2008, ApJ, 682, L73
Smith, G. P., Treu, T., Ellis, R. S., Moran, S. M., & Dressler, A. 2005a, ApJ, 620, 78
Smith, R. J., Lucey, J. R., & Hudson, M. J. 2007, MNRAS, 381, 1035
Soifer, B. T., Neugebauer, G., & Houck, J. R. 1987, ARA&A, 25, 187
Springel, V., et al. 2005, Nature, 435, 629
Treu, T., et al. 2003, ApJ, 591, 53
van der Wel, A., et al. 2007, ApJ, 670, 206
Wake, D. A., Collins, C. A., Nichol, R. C., Jones, L. R., & Burke, D. J. 2005, ApJ, 627, 186
Werner, M. W., et al. 2004, ApJS, 154, 1
Wolf, C., Gray, M. E., & Meisenheimer, K. 2005, A&A, 443, 435
Zhang, Y.-Y., Finoguenov, A., Böhringer, H., Kneib, J.-P., Smith, G. P., Kneissl, R., Okabe, N., & Dahle, H. 2008, A&A, 482, 451
Zheng, X. Z., et al. 2007, ApJ, 661, L41